Chapter 4

VISUALIZING PATHOGENIC PROTEIN SYNTHESIS DURING INFECTION

4.1 Abstract

We extend cell-selective bioorthogonal noncanonical amino acid tagging (BONCAT) to visualize staphylococcal protein synthesis in three dimensions within skin abscesses. We use BONCAT methodology combined with the hybridization chain reaction (HCR) to visualize both proteins and rRNA within cleared abscesses. We hypothesize that this methodology can be readily applied to diverse microbial systems to study the biogeography of host-microbe interactions.

This work was a collaboration with Will H. DePas, Bryan Yoo, Sarkis K. Mazmanian, and Dianne K. Newman.

4.2 Introduction

The biogeography, or spatial arrangement of microbes within a host, depends on the features of their microenvironment such as nutrient availability, oxygen levels, and host-cell interactions. Characterizing these spatial arrangements is important to understanding and controlling microbes as they interact with the host (1, 2). While thin sectioning of abscesses has led to remarkable insights into host-microbe interactions, tools to study the three-dimensional biogeography of infection are currently limited. Using tissue-clearing techniques to visualize infection may produce insights previously unobtainable by thin slicing alone.

Recent advances in tissue clearing techniques such as the passive CLARITY technique (PACT) have been used to render tissues transparent and allow for visualization of fine structure in three-dimensions (3). Importantly, PACT preserves the spatial relationships of molecules within the cell by encasing them within an acrylamide-based hydrogel, and is compatible with most immunohistochemistry or *in situ* hybridization techniques (4-6). While most researchers using PACT have focused on neuroscience applications due to the method's ability to preserve neural structure within the brain, the Tobin lab has used PACT to visualize granulomas of *Mycobacterium tuberculosis* expressing a fluorescent protein in clarified murine lung tissue and whole zebrafish (7, 8).

Recently, the Newman lab developed the microbial identification after passive CLARITY technique (MiPACT) to study polymicrobial infections within sputum samples from

patients with cystic fibrosis (CF) (9). This method uses hybridization chain reaction (HCR) to identify and visualize microbial species by labeling their ribosomal RNA (rRNA). HCR uses short DNA probes complementary to a target RNA to trigger the polymerization of fluorophore-labeled DNA hairpins in a hybridization chain reaction, effectively amplifying signal from *in situ* hybridization (10, 11). By using HCR and PACT, they were able to both quantify growth rates of CF pathogens and visualize substructures of multi-community biofilms in sputum.

We hypothesized that cell-selective bioorthogonal noncanonical amino acid tagging (BONCAT) could be used with tissue-clearing to explore both the protein localization and substructures formed by *Staphylococcus aureus* during skin infection. In this chapter, we apply MiPACT to staphylococcal abscesses that have been cell-selectively labeled using BONCAT to visualize both pathogenic proteins and rRNA during infection.

4.3 Results

Staphylococcal abscesses can be clarified using PACT. As detailed in Chapter 3, we first labeled proteins synthesized by methicillin-resistant *Staphylococcus aureus* (MRSA) within murine skin abscesses using azidonorleucine (Anl) (Fig 4.1A). After excision and fixation of the abscess, we tested various ratios of bisacrylamide, acrylamide, and paraformaldehyde (PFA) for embedding conditions to encase the skin abscess within a stabilizing hydrogel. The conditions we settled on were 4% of a 29:1 acrylamide:bis-acrylamide (v/v) mixture, 1% paraformaldehyde (PFA), and 0.25% of the thermal-initiator VA-044 in 1X PBS, which we called “B4P1”.

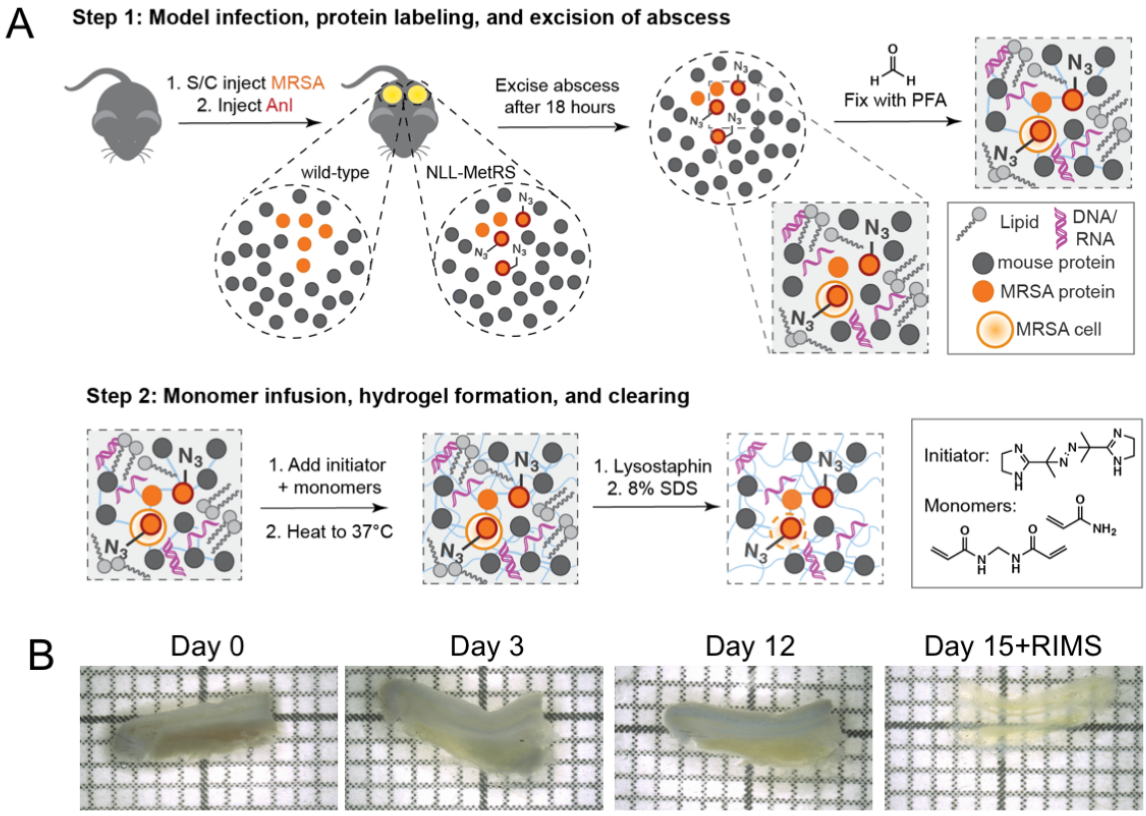

Figure 4.1: A) Scheme used to label skin abscess during infection, embed within hydrogel, and remove lipids. B) Pictures of the abscess during incubation in SDS and after submersion in refractive index matching solution (RIMS). Each square represents 1 mm^2.

Other conditions tested, with smaller quantities of bisacrylamide or PFA were less robust to the subsequent protocols: the inner staphylococcal abscesses would often separate from the epidermal layer. After polymerization, we cut the abscess into ~1 mm thick slices and removed the lipids from the tissue using the passive clarity technique (PACT). We took pictures of these skin abscess pieces over 15 days to monitor clearing (Fig 4.1B). We did not notice additional clearing after day 12, and on day 15 we resuspended the tissue in refractive index matching solution (RIMS) for 24 hours. The skin abscess appeared

significantly more transparent (Fig 4.1B). Collagenase treatment prior to clearing steps did not show enhanced transparency.

BONCAT/HCR labeling is compatible with PACT. To determine optimal click chemistry and HCR conditions to use on the skin abscesses, we first tested several conditions on B4P1 hydrogel blocks of *S. aureus* +MetRS or –MetRS strains grown in tryptic soy broth (TSB) and labeled with azidonorleucine (Anl) for 1 hour during mid-exponential growth. We tested the copper-catalyzed alkyne-azide cycloaddition (CuAAC) with a terminal alkyne-functionalized tetramethylrhodamine (TAMRA) or the strain-promoted alkyne-azide cycloaddition (SPAAC) using aza-dibenzocyclooctyne functionalized with TAMRA, before and after processing the samples with HCR probes. We found that the only conditions that showed signal from both the click reaction and HCR was when we performed the click reaction first using SPAAC, followed by a washing step, then incubation with HCR probes (Fig S4.1, Fig 4.2A).

We then took the azide-tagged and clarified skin abscess pieces, performed SPAAC with DBCO-TAMRA, then performed HCR with 30 nM staphylococcal-specific initiator probe (STA3) and corresponding amplification hairpins tagged with AlexaFluor488 (120 nM, B4-AF488). After washing unbound probes away followed by 24 hours of incubation in RIMS, we visualized abscesses and saw signal for both ribosomal RNA and newly-synthesized proteins within the abscess (Fig 4.2C). Probes with a "mismatch" sequence (no complementarity to target RNA) showed little background signal in the AF488

channel (Fig S4.2A) and samples infected with a –MetRS strain showed no signal in the TAMRA channel (Fig 4.2B), suggesting that the signal was specific. First attempts to stain skin abscesses showed a high degree of background labeling in the thick epidermal layer, but this signal was decreased by adding 1 µM of a random DNA primer to the hybridization step, effectively blocking charged regions that nonspecifically bind the DNA probes within the tissue.

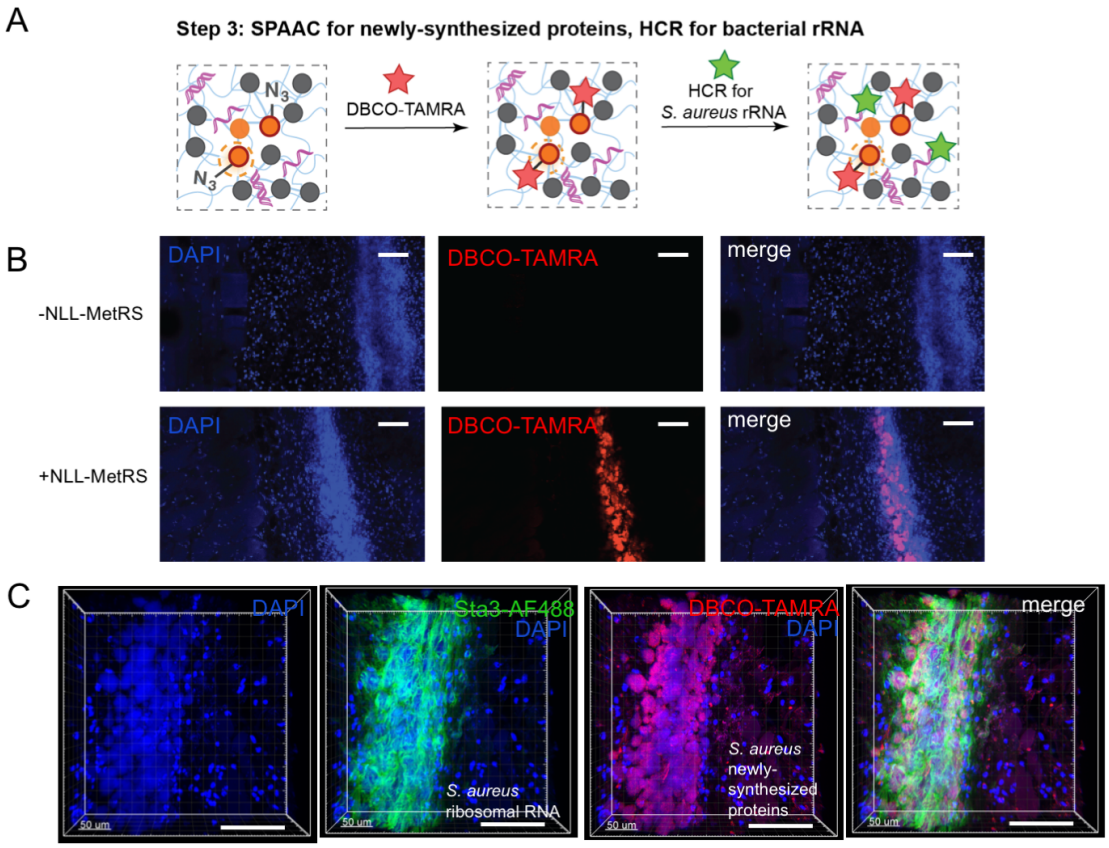

Figure 4.2: A) Scheme used to conjugate DBCO-fluorophore to newly synthesized proteins, followed by HCR for *S. aureus* ribosomal RNA (rRNA). B) Fluorescence microscopy of skin abscess pieces (volume ~30 mm^3) after following steps described in Fig 4.1A and 4.2A. Scale bars are 100 µm. C) Staining for azide-tagged proteins (red) overlaid in three-dimensional space with HCR for staphylococcal rRNA.

Notably, the colocalization of the HCR signal and the BONCAT signal was inconsistent: though the two signals did appear in the same general area of the abscess, their spatial arrangement and patterns were markedly different. This implied that the newly synthesized azide-tagged staphylococcal proteins were not in the same location as the rRNA used to synthesize them. In several experiments the rRNA probes appeared to surround the staphylococcal proteins in a fibrous “halo”, while in others the HCR signal appeared offset from the bulk of the MRSA abscess as visualized through BONCAT and DAPI. (Fig 4.2C). This result was puzzling, as we had expected the HCR signal to appear as puncta colocalized with protein visualization. We repeated the experiment but swapped the fluorophore used so that SPAAC was performed using DBCO-AF488 and the HCR amplification hairpins were conjugated to AlexaFluor647 (AF647). We again saw the HCR signal for staphylococcal rRNA slightly offset from the newly-synthesized staphylococcal proteins visualized with BONCAT (Fig 4.3).

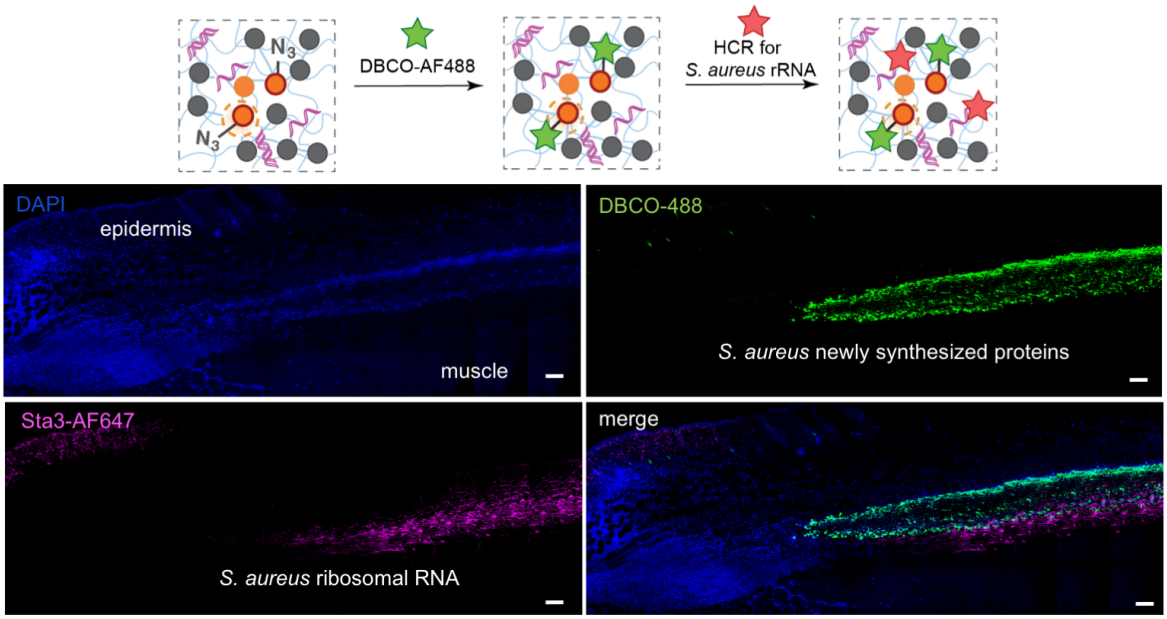

Figure 4.3: Wider field view of skin abscess following a similar protocol to Fig 4.2 except with different fluorophores. Scale bars are 100 µm.

Comparison of BONCAT/HCR labeling using PACT with thin sections. We aimed to compare the biogeography observed with PACT to that observed with traditional thin sectioning techniques. We cryosectioned fixed Anl-labeled staphylococcal abscesses to ~15 µm thick before applying BONCAT and HCR probes. Similar to the PACT results, we observed that the HCR signal colocalized only partially with the BONCAT signal. Furthermore, in the cryosectioned samples there was a strong BONCAT signal showing newly-synthesized staphylococcal proteins in a deeper layer of the skin abscess that we had previously not observed in the PACT samples (Fig 4.4). This BONCAT signal colocalized perfectly with polyclonal anti-*S. aureus* immunostaining, confirming the identity of staphylococcal proteins. We also compared these microscopy images to hematoxylin and eosin-stained (H&E) paraffin slices (~10 µm), in which the abscess

demonstrates a dark purple color due to the large amount of polymorphonuclear leukocytes (neutrophils, or PMNs) (Fig 4.4).

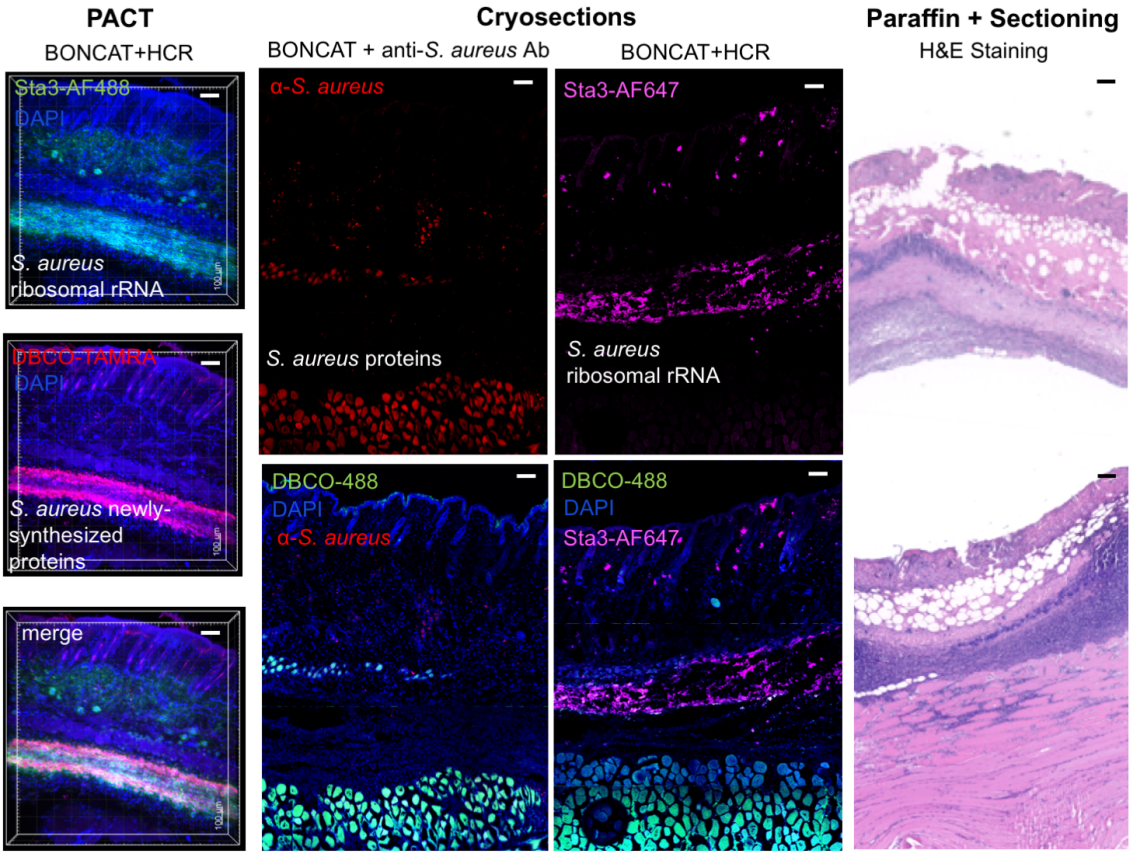

Figure 4.4: Comparisons of various techniques to visualize staphylococcal skin abscesses. Scale bars are 100 μm. In the samples cleared by PACT (~3x3x3 mm in volume), the HCR signal surrounded the BONCAT signal. In the cryosections, a similar pattern was seen to the PACT samples in the top portion of the skin (towards the epidermis), but an additional strong BONCAT signal (DBCO-488) was seen in the lower layers of the skin (towards the muscle). Additionally, the BONCAT signal for newly-synthesized proteins overlays with an anti-*S. aureus* polyclonal antibody. After paraffin embedding, thin-sectioning, and H & E staining, the neutrophils (dark purple) can be seen in several layers of the abscess within the skin.

4.4 Discussion and Future Directions

The colocalization of the anti- *S. aureus* immunostaining with signal from BONCAT suggests we have successfully tagged newly-synthesized staphylococcal proteins within the skin. HCR results are less clear as they do not exactly colocalize with signal from *S. aureus* proteins within this skin abscess infection model.

We have several testable hypotheses as to why part of the abscess lacked HCR signal: 1) the rRNA in this area is being degraded prior to detection, 2) the BONCAT and immunostaining is visualizing lysed *S. aureus* within host phagocytes, 3) the BONCAT and immunostaining is visualizing secreted proteins from *S. aureus*. During skin infection, *S. aureus* secretes numerous toxins to lyse host cells, sometimes while within phagocytes (12, 13), and BONCAT has previously been shown to tag secreted proteins (14). Chatterjee *et al*. showed that ~60% by mass of the proteins secreted by a S. aureus *in vitro* culture was a class of toxins known as phenol soluble modulins (PSMs) (15). Further immunohistochemistry experiments using antibodies against these toxins could confirm the identity of potential proteins secreted into the abscess.

Additional RNA preservation steps (RNase inhibitors, for example) may be required for these hydrogel-embedded tissues. However, because the HCR signal was similar in both cleared tissues and cryoslices, we reasoned that penetration of the DNA probes in the abscess is not the issue, even within the dense hydrogel network. The strong BONCAT signal colocalized with anti-*S. aureus* immunostaining in the area not labeled by HCR was only seen in the cryoslices, and not in the clarified skin tissue. Future experiments could

elucidate whether this is because the hydrogel-embedded tissue is losing this part of the abscess, or if the clearing step is removing some newly-synthesized tagged proteins. Increased amounts of bisacrylamide and PFA may lend increased stiffness to the skin layers to preserve the intact abscess, but decreasing the hydrogel porosity may reduce probe penetration and increase artifacts such as swelling.

While tissue-clearing processes such as PACT have not reported on the loss of large amounts of proteins before, it is known that fluorescent lipophilic molecules like DyeI (MW: ~1 kDa) are incompatible with these techniques as they associate with the lipids removed from cell membranes. Several secreted staphylococcal toxins such as PSMs and the related delta-toxin are small (2-3 kDa), detergent-like cytolytic proteins that associate with host cell membranes and form transient pores within the membrane (16). It is possible that the tissue clearing detergents used in PACT remove this class of proteins, potentially revealing a limitation to this method in the visualization of pathogenic proteins in host tissue. We could test this hypothesis by assaying the PACT solution post clearing for proteins using Western blotting or LC-MS/MS (4).

We have shown the chemistries used for conjugation of azide-tagged molecules are compatible with the HCR and PACT techniques pioneered by MiPACT. We envision cell-selective labeling using BONCAT could be combined with tissue-clearing techniques to not only visualize host-pathogen interactions, but neural proteomic mapping as well.

4.5 Supplementary Information

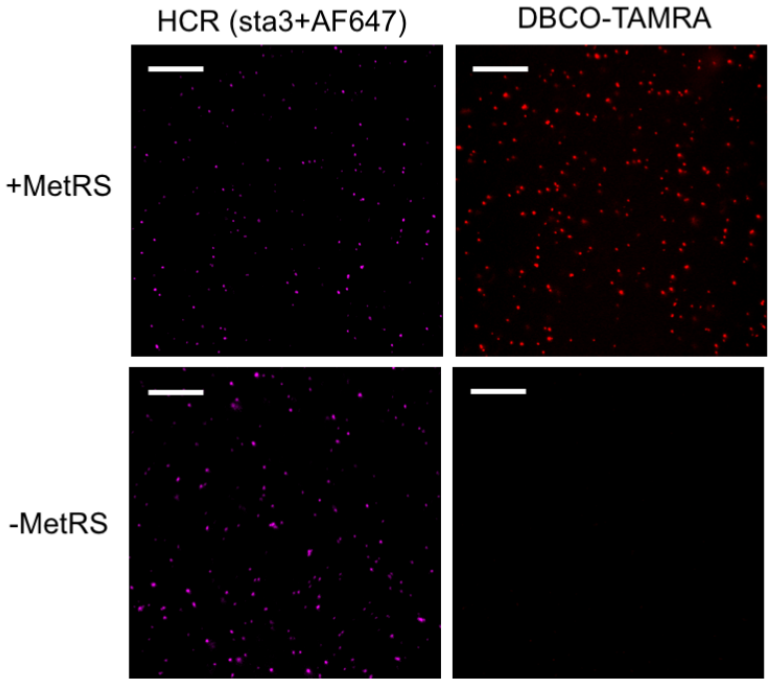

Supplemental Figure S4.1 DBCO-TAMRA labeling of incorporated azides and HCR staining for *S. aureus* in B4P1 hydrogels. Only the +MetRS samples show signal in the DBCO-TAMRA channel, while both the –MetRS and +MetRS samples show HCR signal for staphylococcal RNA. Scale bars are 50 µm.

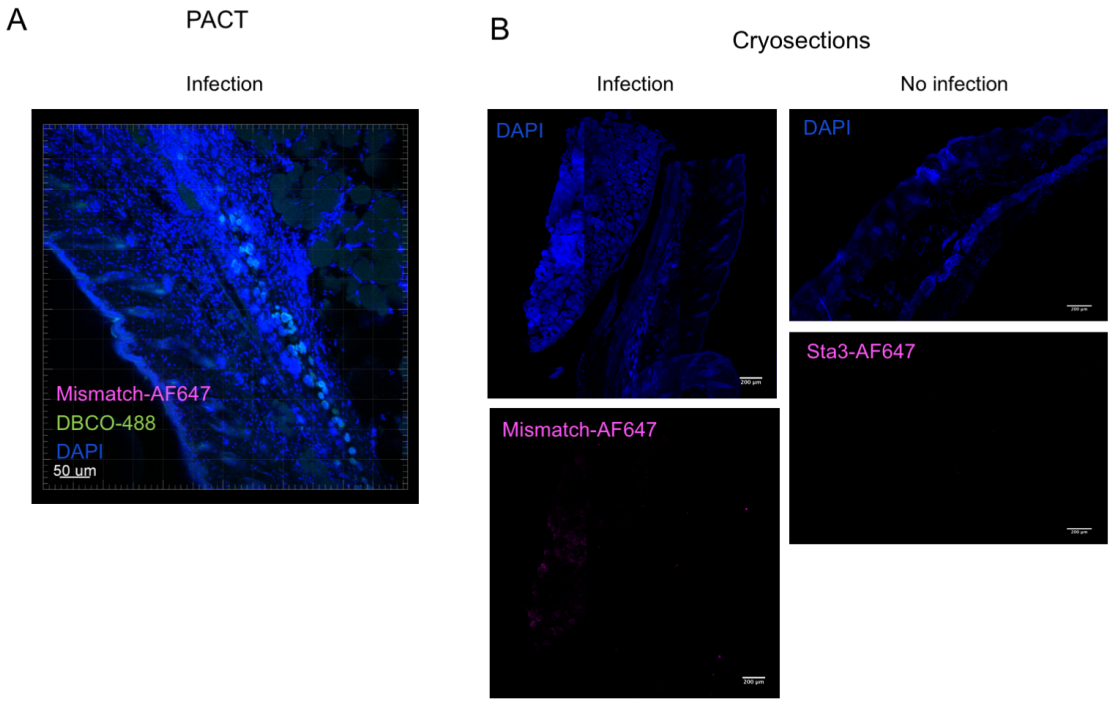

Supplemental Figure S4.2: Controls for HCR in A) PACT abscesses and B) cryoslices. Mismatch-RNA probes show no binding to the abscess and staphylococcal probes do not bind to uninfected skin.

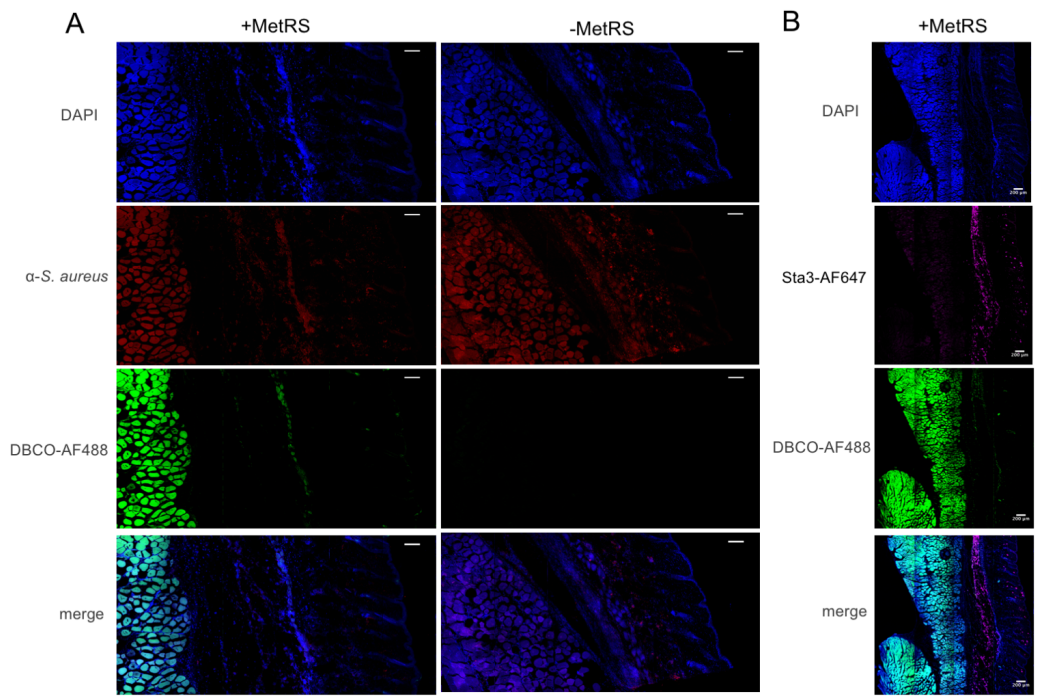

Supplemental Figure S4.3 A) BONCAT signal overlays with α-*S. aureus in* cryoslices. Only samples with +MetRS show signal in the DBCO-AF488 channel, while both +MetRS and MetRS samples stain positively for *S. aureus* proteins using an anti-*S. aureus* antibody. B) Staphylococcal rRNA signal does not entirely colocalize with BONCAT signal.

Experimental Procedures

Strains and growth conditions. The following strains were used in this study: *Staphylococcus aureus* USA300, JE2 (NARSA), grown in tryptic soy broth (TSB) aerobically with shaking at 250 rpm.

Embedding labeled bacteria grow*n in vitro* in hydrogel blocks. We used similar procedures as DePas *et al* with slight modifications. (9). *S. aureus* strains –MetRS (pWW412, see Appendix A) or +MetRS (pSS20_hprk, see Appendix A) were inoculated from single colonies from tryptic soy agar (TSA) plates in TSB with chloramphenicol (20

μg/mL). When the cultures reached mid-exponential phase, 2 mM of azidonorleucine (Anl) was added for 1 hour. The cultures were washed with PBS, and fixed overnight at 4 °C in 4% paraformaldehyde (PFA). Fixed samples were resuspended in 29:1 acrylamide:bis-acrylamide (v/v) (Bio-Rad 161-0146) and 0.25% VA-044 hardener (w/v) (Wako 27776-21-2) in 1X PBS for polymerization. After removing oxygen from the solution in an anaerobic chamber, blocks were polymerized at 37 ºC for three hours, without shaking, and then cut to ~3 mm^3. The staphylococcal cells were then digested with lysostaphin (50 μg/mL) in 50 mM Tris buffer for 2 hours at 37 °C. Samples were washed twice in PBS, then "cleared" for 5 days in 8% SDS in PBS at 37 °C.

Ethics statement. Animal experiments were performed in accordance with the regulations for the Institutional Animal Care and Use Committee (IACUC) at Caltech.

Embedding murine skin abscesses in hydrogel blocks. *S. aureus* strains -MetRS or +MetRS were prepared as described in Chapter 3 for skin infection. After labeling with Anl for 16 hours, the mice were culled (CO_2) and the abscesses excised. They were directly added to 4% paraformaldehyde (PFA) for fixation overnight at 4 °C then washed with PBS. Fixed samples were resuspended in 29:1 acrylamide:bis-acrylamide (v/v) (Bio-Rad 161-0146) 1% paraformaldehyde (PFA, EMS #15713), and 0.25% VA-044 hardener (w/v) (Wako 27776-21-2) in 1X PBS for polymerization. The staphylococcal cell wall was then digested with lysostaphin (50 μg/mL) in 50 mM Tris buffer for 6-12 hours at 37

°C. Samples were washed once in PBS, then cleared for 5-21 days in 8% SDS in PBS at 37 °C.

Click Reaction. After washing the SDS out of the cleared samples with three washes of PBS, free cysteines were blocked with 100 mM iodoacetamide in PBS at room temperature for 4-16 hours. Oftentimes, samples are reduced prior to blocking, but using 10 mM dithiothreitol (DTT) before iodoacetamide treatment showed higher background labeling. DBCO-TAMRA or DBCO-AF488 (Click Chemistry Tools) was added to a fresh solution of 100 mM iodoacetamide to a concentration of 5 μM and the reaction proceeded for 1 hour. The samples were washed twice in PBS (30 min each), rotated end over end in 50% DMSO in PBS overnight, then washed three more times in PBS.

HCR. 5'-ATTTCACATTTACAGACCTCAACCTACCTCCAACTCTCAC-3' was added to the 3' end of the DNA probe (termed "B4" (10)). DNA hairpins (Molecular Instruments) conjugated to either AlexaFluor-488 or AlexaFluor-647 as indicated were used with the appropriate initiator probe sets.

We initially used a previously-reported STA3 probe (17), but found high signal-to-noise with this sequence, so we increased the length of our probe from 16 nucleotides to 31 nucleotides. Microscopy images of the HCR in abscesses were all performed with this STA3_long probe. Sequence in Supplementary Table 1.

Hybridization: Samples were hybridized in 500 µL of HCR hybridization buffer (100 µL of 20X SSC, 100 mg dextran sulfate (Sigma D6001), 250 µL formamide, ddH_2O to 1 mL) with 30 nM initiator probe at 46 ºC, with shaking, for 24-48 hours. All solutions were filter sterilized. Excess probe was removed by washing each sample in 50 mL 84 mM FISH wash buffer (840 µL of 5 M NaCl, 1 mL of Tris-HCl [pH 7.6], 500 µL of 0.5 M EDTA [pH 7.2], 100 µL of 5% SDS, and Milli-Q H_2O to 50 mL) at 52 °C for 6 hours in a water bath.

Amplification: Hairpin pairs were first heated at 95 °C for 90 seconds in a thermocycler in separate PCR tubes, then cooled at room temperature for 30 minutes. Each hairpin in a pair was added to a final concentration of 115 nM. Amplification buffer with the appropriate hairpin mixture (120 µL) was then added to each sample in a 1.5 mL centrifuge tube. Samples were incubated at room temperature with gentle shaking for 24-48 hours. After amplification, samples were washed in 337.5 mM FISH wash buffer (3375 µL of 5 M NaCl, 1 mL of Tris-HCl [pH 7.6], 500 µL of 0.5 M EDTA [pH 7.2], 100 µL of 5% SDS, and Milli-Q H_2O to 50 mL) at 48 °C for 3 hours in a water bath. Samples were then incubated in 250 µL RIMS with 10 µg/mL DAPI (1:1000 from 10 mg/mL stocks in DMSO) at room temperature for at least 16 hours before imaging.

Microscopy. Prior to imaging, samples were incubated at RT, with shaking, overnight in RIMS with 1 µg/mL DAPI. Samples were then mounted on slides in 0.9 mm or 1.7 mm Coverwell perfusion chambers (Electron Microscopy Services) with a coverslip on the top. Imaging was performed using a Zeiss LSM 880 confocal microscope with a Plan-

Apochromat 10x/0.45 M27 objective (WD 2.0 mm). All images and Z-stacks were collected in 12-bit mode, with at least 1024x1024 scan format. Images were processed using Imaris imaging software (Bitplane) or the FIJI distribution of ImageJ (18).

Histological examination of mouse skin abscesses. Mouse skin was harvested 2 days after inoculation and fixed in 10% neutral-buffered formalin for 48 hours. Fixed tissues were embedded in paraffin, sectioned (5 μm), mounted on slides, and stained with hematoxylin and eosin (Pacific Pathology).

Cryosectioning, DBCO-staining, immunostaining, and imaging. Abscesses were excised, placed in optimum cutting temperature (O.C.T.) compound, and frozen at -80 °C. They were then cut into ~15 μm sections and deposited onto glass slides. The slides were fixed with 2% paraformaldehyde (PFA), permeabilized with 0.1% Triton-X, and treated with lysostaphin at 37 °C. The samples were next blocked in 100 mM iodoacetamide for 30 min in the dark, then reacted with 5 μM DBCO-AlexaFluor488 (Click Chemistry Tools) for 15 min. After washing, the samples were blocked with 1% mouse serum, then treated with a 1:3000 dilution of anti-*Staphylococcus aureus* antibody (polyclonal, rabbit) (Ab37644, Abcam). A goat anti-rabbit secondary antibody conjugated to AlexaFluor555 (Thermo Scientific) was then added at 1:10,000 dilution. Samples were washed with PBS, and Vectashield Antifade with DAPI was added prior to coverslips. Imaging was performed using a Zeiss LSM 880 confocal microscope with a Plan-Apochromat 10/0.45-

numerical aperture M27 objective (WD 2.0 mm) or a 25X objective. Image reconstruction and analysis was performed in the FIJI distribution of ImageJ (18).

Supplemental Table 1: Probes used in this study:

Species	Name	Sequence
Staphylococcus	STA3 (17)	GCACATCAGCGTCAGT
Staphylococcus	STA3_long	GATCCCCACGCTTTCGCACATCAGCGTCAGT
-	Mismatch	ACTCCTACGGGAGGCAGC
-	Random	AGCAGGTCGAACTCCTTGAG

References

1. Stacy A, McNally L, Darch SE, Brown SP, & Whiteley M (2016) The biogeography of polymicrobial infection. *Nat Rev Microbiol* 14(2):93-105.
2. Jorth P, *et al*. (2015) Regional Isolation Drives Bacterial Diversification within Cystic Fibrosis Lungs. *Cell Host Microbe* 18(3):307-319.
3. Lai HM, Ng WL, Gentleman SM, & Wu W (2017) Chemical Probes for Visualizing Intact Animal and Human Brain Tissue. *Cell Chem Biol* 24(6):659-672.
4. Chung K, *et al*. (2013) Structural and molecular interrogation of intact biological systems. *Nature* 497(7449):332-7.
5. Yang B, *et al*. (2014) Single-Cell Phenotyping within Transparent Intact Tissue through Whole-Body Clearing. *Cell* 158(4):945-958.
6. Shah S, *et al*. (2016) Single-molecule RNA detection at depth by hybridization chain reaction and tissue hydrogel embedding and clearing. *Development* 143(15):2862-2867.
7. Cronan MR, *et al*. (2016) Macrophage Epithelial Reprogramming Underlies Mycobacterial Granuloma Formation and Promotes Infection. *Immunity* 45(4):861-876.
8. Cronan MR, *et al*. (2015) CLARITY and PACT-based imaging of adult zebrafish and mouse for whole-animal analysis of infections. *Dis Model Mech* 8(12):1643-1650.
9. DePas WH, *et al*. (2016) Exposing the Three-Dimensional Biogeography and Metabolic States of Pathogens in Cystic Fibrosis Sputum via Hydrogel Embedding, Clearing, and rRNA Labeling. *Mbio* 7(5): e00796-16.
10. Choi HMT, Beck VA, & Pierce NA (2014) Next-Generation *in Situ* Hybridization Chain Reaction: Higher Gain, Lower Cost, Greater Durability. *ACS Nano* 8(5):4284-4294.
11. Dirks RM & Pierce NA (2004) Triggered amplification by hybridization chain reaction. *Proc Natl Acad Sci* 101(43):15275-15278.

12. Thurlow LR, *et al*. (2013) Functional Modularity of the Arginine Catabolic Mobile Element Contributes to the Success of USA300 Methicillin-Resistant *Staphylococcus aureus*. *Cell Host Microbe* 13(1):100-107.
13. Li M, *et al*. (2010) Comparative analysis of virulence and toxin expression of global community-associated methicillin-resistant *Staphylococcus aureus* strains. *J Infect Dis* 202(12):1866-1876.
14. Mahdavi A, *et al*. (2014) Identification of secreted bacterial proteins by noncanonical amino acid tagging. *Proc Natl Acad Sci* 111(1):433-438.
15. Chatterjee SS, *et al*. (2013) Essential *Staphylococcus aureus* toxin export system. *Nat Med* 19(3):364-367.
16. Otto M (2014) *Staphylococcus aureus* toxins. *Curr Opin Microbiol* 17:32-37.
17. Tavares A, Inacio J, Melo-Cristino J, & Couto I (2008) Use of fluorescence *in situ* hybridization for rapid identification of staphylococci in blood culture samples collected in a Portuguese hospital. *J Clin Microbiol* 46(9):3097-3100.
18. Schindelin J, *et al*. (2012) Fiji: an open-source platform for biological-image analysis. *Nat Methods* 9(7):676-682.